PCCP
Physical Chemistry Chemical Physics

Accepted Manuscript

This article can be cited before page numbers have been issued, to do this please use: A. Atila, S. Ouaskit and A. Hasnaoui, *Phys. Chem. Chem. Phys.*, 2020, DOI: 10.1039/D0CP02910F.

ROYAL SOCIETY OF CHEMISTRY

rsc.li/pccp

View Article Online
DOI: 10.1039/D0CP02910F

PCCP

ARTICLE TYPE

Cite this: DOI: 00.0000/xxxxxxxxxx

Ionic Self-Diffusion and the Glass Transition Anomaly in Aluminosilicates†

Achraf Atila,*[a] Said Ouaskit,[b] and Abdelatif Hasnaoui[c]

Received Date
Accepted Date

DOI: 00.0000/xxxxxxxxxx

The glass transition temperature (T_g) is the temperature, after which the supercooled liquid undergoes a dynamical arrest. Usually, the glass network modifiers (e.g., Na_2O) affect the behavior of T_g. However, in aluminosilicate glasses, the effect of different modifiers on T_g is still unclear and show an anomalous behavior. Here, based on molecular dynamics simulations, we show that T_g decreases with increasing charge balancing cations field strength (FS) in the aluminosilicate glasses, which is an anomalous behavior as compared to other oxide glasses. The results show that the origins of this anomaly come from the dynamics of the supercooled liquid above T_g, which in turn is correlated to pair excess entropy. Our results deepen our understanding of the effect of different modifiers on the properties of the aluminosilicate glasses.

1 Introduction

The aluminosilicate glasses are of great interest in glass science and industry. This is due to their good physical properties and chemical stability, without neglecting the abundance of the glass elements in the earth's crust[1–3]. The glass transition temperature is a vital glass property when considering glasses for a specific application. T_g is the temperature; below it, the physical properties of the supercooled liquid change to those of a glassy state presenting rigidity and elasticity due to the structural dynamical arrest. Knowing which factors control T_g and how different modifiers affect the values of T_g will deepen our physical and chemical understanding of the behavior of the glass transition.

Cation field strength (FS) as defined by Dietzel[4] FS = $Z_X/(r_X+r_O)^2$, where Z and r stand for the charge and ionic radius, respectively, and indicates the cation-oxygen bond strength (higher FS means higher bond strength). This parameter could be used to study the effect of different modifiers or charge balancing cations on the properties of oxide glasses. Based on this assumption, it is expected that the properties of the studied oxide glasses to scale with FS. Moreover, the oxygen ionic radius is omitted from the FS equation, as it is approximated to be the same (FS = $\frac{Z_X}{r_X^2}$).

The properties of oxide glasses such as T_g, hardness, and elastic moduli of binary alkali tellurite[5–8], phosphates[9], and ternary alkali/ alkaline earth aluminoborate glasses[10,11] indeed scales with FS. These results suggested that the physical properties of the oxide glasses depend strongly on the charge balancing cations field strength. Furthermore, it has been found that the elastic properties increase with increasing cations field strength in binary alkali silicate glasses[12]. Recently, we have highlighted the same effect in ternary alkali and alkaline earth aluminosilicate glasses[3]. Moreover, we showed that the behavior of T_g does not correlate positively with FS and thus showing an anomalous behavior as compared to the previously mentioned glasses. This anomalous behavior of T_g observed from our previous MD simulations[3] was already found experimentally by Weigel *et al.*[13]. Moreover, this behaviour was also observed by Pedone *et al.*[12] and showed previously by some of us[14] in binary silicate glasses where the alkali and alkaline earth cations act as modifiers rather than charge balancing. The anomalous behavior of T_g is still not explained in the literature and remains unclear. The glasses contain either monovalent alkali cation, divalent alkaline earth cations, or Zn. To harness this effect, we simulated eight charge-balanced aluminosilicate glasses using molecular dynamics (MD) simulations, which offers a powerful tool for investigating and understanding the atomic-scale behavior of materials.

Here, we show that the origins of the anomalous behavior of T_g lies in the diffusion behavior of the charge balancing cations and to a less extend to the degree of the ordering in the glasses. The glasses contain either monovalent alkali cation, divalent alkaline earth cations, or Zn. The content of the modifier was set to be equal to that of alumina giving a ratio R=1 ($R=[X^{n+}_{2/n}O]/[Al_2O_3]$)[3,15]. Based on these assumptions, the mod-

[a] *Friedrich-Alexander-Universität Erlangen-Nürnberg, Materials Science and Engineering, Institute I, Martensstr. 5, Erlangen 91058, Germany.*
[b] *Laboratoire de Physique de la Matière Condensée, Faculté des Sciences Ben M'sik, University Hassan II of Casablanca, B.P 7955, Av Driss El Harti, Sidi Othmane, Casablanca, Maroc.*
[c] *LS3M, Faculté Polydisciplinaire Khouribga, Sultan Moulay Slimane University of Beni Mellal, B.P 145, 25000 Khouribga, Morocco*
* Corresponding author: achraf.atila@fau.de
† Electronic Supplementary Information (ESI) available: See DOI:

View Article Online
DOI: 10.1039/D0CP02910F

ifiers are expected to behave similarly in the aluminosilicate glasses network (to charge balance tetrahedral AlO^4 units), although, the charge balancing ability will be different (due to the difference in the size of the cations) as the same charge is distributed over a larger area for larger cations.

2 Methods

In this work, eight charge-balanced aluminosilicate glasses $(X^{n+}_{n/2}O)_{25}$-$(Al_2O_3)_{25}$-$(SiO_2)_{50}$ (X stands for Li, Na, K, Mg, Ca, Sr, Ba, or Zn) were simulated using classical molecular dynamics. The well-established potential by Pedone *et al.* [16] was used to model the interactions between atoms. This potential gives a realistic agreement with available experimental data, as mentioned in the literature [3,12,17–19]. Potential parameters and partial charges are given in the reference [16]. All simulations were performed using the large-scale atomic/molecular massively parallel simulator LAMMPS [20]. Velocity-Verlet algorithm with an integration time step of 1 fs was used to integrate the equations of motion. Periodic boundary conditions (PBC) are applied in all directions to avoid edge effects and to simulate bulk systems. Long-range interactions were evaluated by the Ewald summation method, with a real-space cutoff of 12.0 Å and precision of 10^{-6}. The short-range interactions cutoff distance was chosen to be 5.5 Å [16].

All systems consist of approximately 4200 atoms placed randomly in a cubic simulation box, ensuring that there is no unrealistic overlap between atoms. First, we equilibrated the systems at a high temperature (T = 5000 K) for 500 ps. This step is needed to ensure that each system loses the memory of its initial configuration. After that, the systems were subsequently quenched linearly from the liquid temperature (T = 5000 K) to room temperature (T = 300 K) with a cooling rate of 10^{12} K/s while keeping the volume fixed. Nosé-Hoover thermostat and barostat were used to control the temperature and pressure. At 300 K, another run for 1 ns and zero pressure in NPT ensemble was performed, and the structural (short- and medium-range structures) and elastic properties were found to be in a realistic agreement with the experimental data as discussed in the reference [3]. Cooling rates used in molecular dynamics are much higher than those used in experiments due to the intrinsic incapability of molecular dynamics to use very low cooling rates. The values of the cooling rate used in the present simulations are usually used in making glasses in MD simulations, and changing these values over an order of magnitude does not affect the physical properties and the short-range structure of the glassy state considerably [3,21].

3 Results

In order to calculate the values of the glass transition temperature, we can plot the variation of some physical, chemical, or thermodynamic properties of the material such as volume V(T) [15,22], total energy E_t(T) [3], or enthalpy H(T) [23] with respect to temperature. The glass transition temperature is then obtained from the slope break between high- and low-temperature variations of that property versus temperature. The glass transition temperature herein was obtained from the slope break between high- and low-temperature variations of the total energy (E_t(T)) versus temperature and an example of sodium aluminosilicate system is given in supplementary materials Fig. S1. Fig. 1 show T_g values as a function of FS obtained in the present simulations together with the experimental values available in ref [13]. As it can be observed, there is a striking qualitative agreement in the behavior of T_g with FS from our simulations and experimental studies. Also, we can see that the T_g values obtained from the simulations are overestimated by around 300 K compared to experiments. This behavior is usually observed in MD simulations and is generally attributed to the very high cooling rates used in the glass preparation using MD [3,15,24–26]. In recent literature, several methods were used to obtain T_g, as indicated previously. Lodesani *et al.* [22] cooled the glass in NPT ensemble and calculated T_g from the variation of the volume with temperature, while Urata [23] considered a quasi-slow quenching (QSQ)) to obtain a stable glass and calculated T_g values using the variation of the enthalpy (and volume) with temperature during the quenching process by preforming different cooling procedures. In the same context, Atila *et al.* [15] compared T_g values obtained from the variation of the volume with temperature to the values obtained by the inherent structure energy method which is in principle similar to the method used by Urata [23]. It was noticed from all these works that the T_g calculated from the variation of the volume with temperature are remarkably higher than the experimental values with significant errors. These differences could be attributed to the cooling rate, system size, potential, and/ or the thermostat/ barostat used in the simulations. Moreover, by using the inherent structure energy or the QSQ method, one can obtain more realistic T_g values, which compares well with the experimental ones. This is because these methods eliminate any contribution coming from the thermostat/barostat, and the system goes to the closest local energy minimum. It is worth stressing that the QSQ method described in the work of Urata [23] is more artificial than other cooling procedures and might result in a glass structure with different microstructure. Besides that, this could also be partially due to the simulation setup used to obtain bulk glass. The usage of PBC leads to an infinite system without any surfaces. Due to the absence of surfaces, the glasses obtained from computer simulations usually undergo a supercooling, thus giving an effective temperature higher than the experimental one [27]. It is also worth stressing that the calculation of the glass transition temperature values is sensitive to the system size and cooling rate. This dependency on the cooling rate and system size will affect only the values of T_g and not its behaviour. The reader could refer to our previous work [3] where we investigated the effect of the cooling rate on the glass properties in the investigated system herein.

The FS increases along the series $K^+ < Na^+ < Li^+$ and $Ba^{2+} < Sr^{2+} < Ca^{2+} < Mg^{2+}$ while FS of Zn^{2+} is equivalent to that of Mg^{2+}. We also observe from Fig. 1 that T_g decreases with increasing FS for both alkali and alkaline earth system, with a more pronounced decrease for alkali aluminosilicate glasses. The variation of T_g as a function of FS is found to follow Li < Na < K, and Zn < Mg < Ca < Ba < Sr. Since the vitrification is a kinetic process where the dynamics of the melts play an important role, we focus in the following on the diffusion behavior at a temperature range above T_g to explain the behavior of T_g. The mean-squared displacement (MSD) given by $MSD = \langle |r(t) - r(0)|^2 \rangle$ was used to

View Article Online
DOI: 10.1039/D0CP02910F

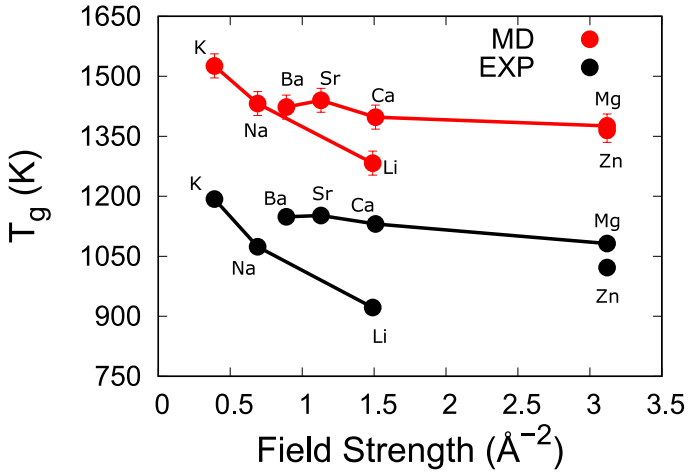

Fig. 1 Glass transition temperature as a function of cations field strength compared with experimental values found in ref[13].

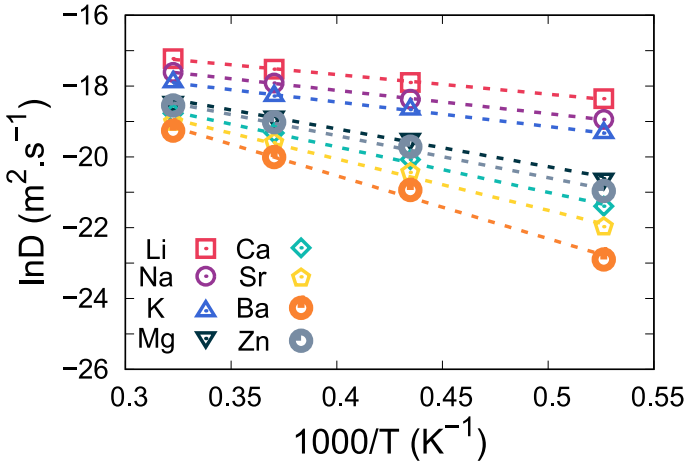

Fig. 2 Diffusion coefficients of Li, Na, K, Mg, Ca, Sr, Ba, and Zn as a function of temperature for the studied aluminosilicate glasses. The symbols represent the simulated data points, and the lines are fit to the Arrhenius law. Error bars are smaller than the symbol size, therefore, they are not shown.

investigate the dynamical properties of the studied system[28]. The MSD was calculated using trajectories under NVT runs for 60 ns and using a time step of 2 fs at each temperature (1900 - 3100 K) (see supplementary materials Fig. S2 - S5), in the beginning of each simulation the sample was relaxed in NPT ensemble at the desired temperature and zero MPa for 50 ps. Fig. S2 - S5 shows that MSD values of network formers are negligible compared to values of alkali ions, we can say that alkali ions migrate rapidly in a quasi-frozen network where Si, Al, and O ions will move slightly or shuffle (compared to alkali ions) to accommodate this fast migration. While alkaline earth ions move in a dynamic network since MSD of network formers (Al, Si, and O) are comparable to MSD of modifiers. The diffusion coefficient D was obtained using Einstein's equation $D = \lim_{t\to\infty}\langle|r(t) - r(0)|^2\rangle/6t$, and averaged over the last 200 ps of each run. The length of the simulation time used in this study is long enough to get a good estimate of the diffusion coefficient. Figure 2 shows the diffusion coefficients D_X (where X stands for charge balancing cations) as a function of temperature in the range between 1900 - 3100 K. The partial diffusion coefficients of O, Si, and Al atoms are shown in supplementary materials Fig. S6.

We see clearly from Fig. 2 that diffusion data follows the Arrhenius behavior $D_X = D_0 exp(-\Delta E_a/k_B T)$ where D_X is the diffusion coefficient of the charge balancing cations, D_0 is the pre-exponential factor, ΔE_a the activation energy barrier for self-diffusion, k_B denotes Boltzmann constant, and T the temperature. The calculated diffusion coefficient from our simulations are in a good agreement with previously reported MD simulations[29–31], and experimental results[32,33]. Also, knowing that the dynamical properties of liquids are very sensitive to the interaction potential[34], the agreement of the data from our simulations with other MD simulations and available experimental data reinforces the reliability of our data. The alkali elements show a higher diffusion as compared to alkaline earth elements in the studied aluminosilicate melts.

Fig. 3(a) and (b) show the variation of the diffusion coefficient as a function of the charge balancing cations field strength at different temperatures. As can be noticed, the self-diffusion coefficient scales with the charge balancing field strength. This behavior could be due to several factors, and to further analyze this behavior, we refer to the entropy. In general, accurate computation of the entropy is extremely costly. Thus, an expression that gives approximately the entropy should be enough to show how different cations can affect the structure of the aluminosilicate melts and glasses. This expression was derived from the expansion of the configurational entropy in terms of multibody correlation functions given by Kirkwood's factorization $S = S_{id} + S_2 + S_3 + ...$, where S_{id} is the ideal gas contribution, S_2 is the pair excess entropy, S_3 is the three-body excess entropy, and other higher terms[35–38]. We use here the term S_2 to take into account only the two-body (pair) excess entropy, which is given by

$$S_2 = -2\pi\rho k_b \int_0^\infty [g(r)lng(r) - g(r) + 1]\, r^2 dr. \qquad (1)$$

ρ is the density of the system and g(r) is the radial distribution function.

The two-body excess entropy is plotted in Fig. 3 (c) and (d) for both alkali and alkaline earth aluminosilicate systems respectively at a temperature range between 1500 - 3100 K. It is worth stressing that higher values of S_2 indicates higher disorder in the system. As depicted in Fig. 3 (c and d) S_2 correlate positively with the charge balancing cations field strength and gives an indication that the systems with high FS cations are more disordered than those with low FS cations.

Additionally, by fitting lnD over 1000/T data to the Arrhenius equation, we can obtain values of the diffusion activation energy barriers ΔE_a and the pre-exponential factor D_0. Although to obtain accurate values of the activation energies and D_0, the temperature range for the fitting should be carefully chosen. The activation energies were obtained by fitting the simulation data to the Arrhenius equation in the temperature range between 1900 and 3100 K.

Figure 4 (a) shows the activation energies for O, Si, and Al self-

View Article Online
DOI: 10.1039/D0CP02910F

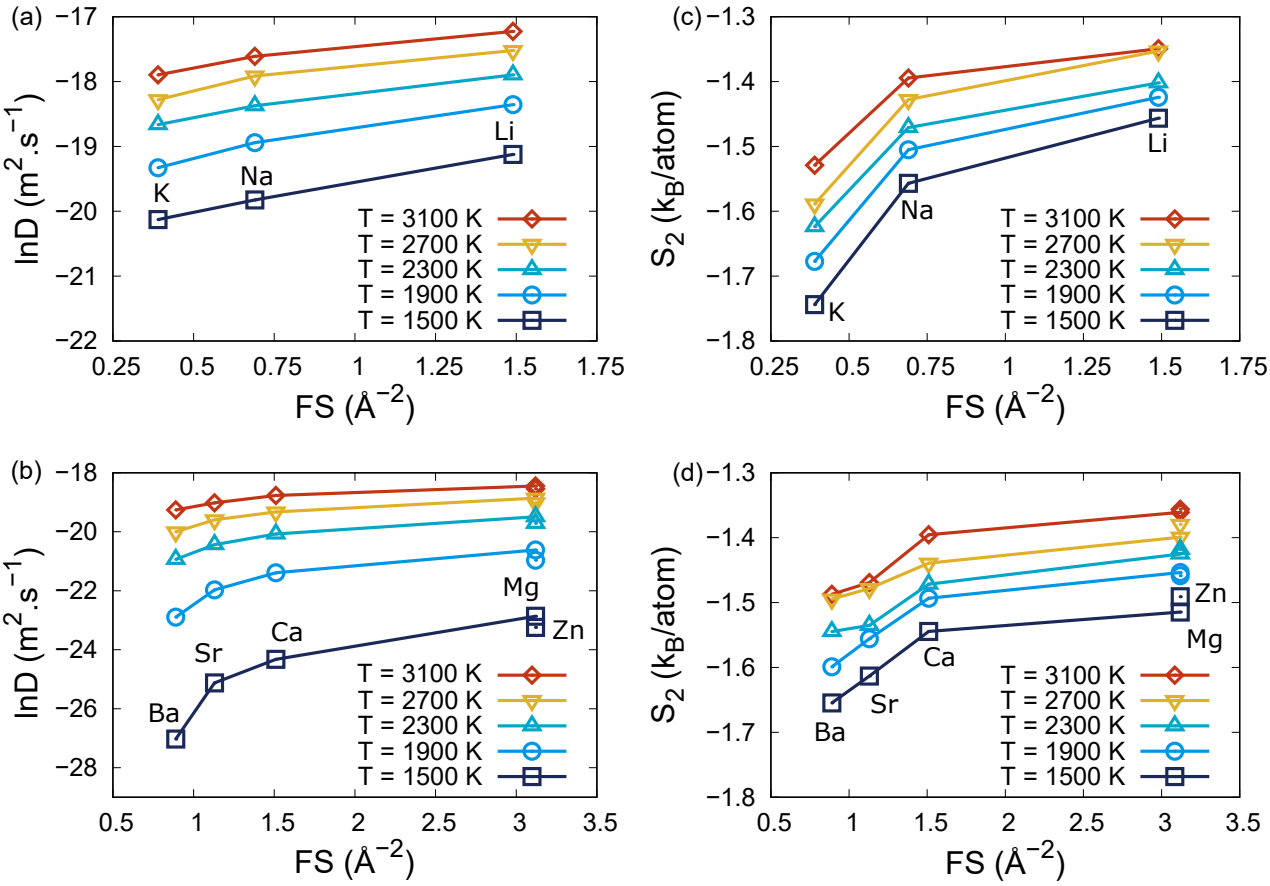

Fig. 3 Diffusion coefficients of Li, Na, K, Mg, Ca, Sr, Ba, and Zn as a function of charge balancing cations field strength for the studied aluminosilicate glasses for different temperatures. (a) shows data for alkali aluminosilicate glasses, and (b) shows data for alkaline earth and Zn aluminosilicate glasses. (c) and (d) show the two-body excess entropy (S_2/N) in the system normalized by the total number of atoms (N) in the system for alkali and alkaline earth aluminosilicate glasses, respectively. The symbols represent the simulated data points, the lines are guide to the eye, and error bars are smaller than the symbol size.

diffusion as a function of FS (see supplementary materials Fig. S7, Table. S1, and Table. S2 for numerical data of E_a and $\ln D_0$ of all elements). The activation energies for the diffusion of O, Si, and Al atoms are shown in supplementary materials Fig. S7.
As we can see, the activation energy decreases with FS for all systems, as expected from the increase of the diffusion coefficient with FS (see Fig. 3). In the same figure, the pre-exponential factor D_0 is also plotted as a function of FS. For the aluminosilicate systems containing alkaline earth or Zn, we noticed a striking similarity in the behavior of D_0 and E_a as a function of FS, while for the aluminosilicate glasses containing alkali cations, D_0 increases with increasing FS.

4 Discussion

For the present glass systems, T_g depends on the FS of the non-network former cations; thus, it depends directly on the radius of the charge balancing cations. The same trends have been reported by Romano *et al.*[39] in the behavior of the viscosity of $XAlSi_3O_8$ melts in the temperature region around T_g, where X stands for (Li, Na, K, $Ca_{0.5}$, $Mg_{0.5}$). It is also known that in aluminosilicate, T—O (T = Si or Al) bonds are the strongest. The introduction of a modifier cation induces a perturbation to these bonds in the form of competition between Si, Al, and X atoms to form bonds with oxygen atoms (X is the non-framework cation). Increasing the field strength of modifying cations leads to an increase of the perturbation in the glass network and increases the probability of the non-framework cations to form bonds with oxygen atoms[3,40].

Furthermore, low FS charge balancing cations enhance the thermal stability of aluminosilicate melt structures. They do not strongly polarize the bridging oxygen and only weakly perturb the aluminosilicate structure. On the contrary, high FS cations form relatively strong bonds with the bridging oxygen that perturb the aluminosilicate structure by narrowing the T—O—T bond angle and lengthening the T—O bonds[3,41].

The higher mobility of the charge balancing cations could be one of the reasons to explain the decrease in the glass transition temperature for the charge-balanced aluminosilicate glasses. The diffusion coefficient scales with field strength as follows; Li > Na > K > Mg > Zn > Ca > Sr > Ba, indicating that atoms which have a higher field strength (e.g., Li, Mg and/ or Zn) diffuse faster than those with lower field strength. The diffusion coefficients of the alkaline-earth aluminosilicate liquids are lower than the corresponding diffusion coefficient of the alkali alumi-

View Article Online
DOI: 10.1039/D0CP02910F

nosilicate liquids. For alkali aluminosilicate melts, the activation energy for self-diffusion decreases with increasing FS while the pre-exponential factor (D_0) shows an increase indicating higher jump frequency of the alkali cation. This is because increasing FS is manifested by a decrease of the cation size leading to lower mobility of the modifier cation. From another side, we noticed that when the FS increases, the coordination number decreases for both alkali and alkaline-earth cations, as shown in Fig. 4 (b) allowing more freedom for low-coordinated cations, which is corroborated by the increase in the diffusion coefficient. As discussed above, alkali cations have higher diffusion coefficients and smaller activation energy barriers, so they are faster and easier to diffuse. The pre-exponential factor D_0 for these elements increases with increasing FS meaning that high FS cations can explore more configurational space and relax towards lower energy minima, thus lowering T_g. As for alkaline earth cations, both the activation energies and D_0 for self-diffusion decreases with increasing FS, indicating that even if the activation energy barriers for self-diffusion are smaller for high FS elements, the jump frequency is lower which lead to slow relaxation of the systems. However, the values of T_g of potassium aluminosilicate glass are higher than T_g of the magnesium aluminosilicate glass. This could be attributed partially to the high coordination state of potassium as compared to magnesium and partially to the cation molar mass (potassium is heavier than magnesium). This fact could also explain the higher T_g values of alkaline earth AS glasses. The low energy barriers for self-diffusion found in those melts give to the systems the freedom to relax more towards lower energy minima resulting in lower T_g values as compared to other systems with lower field strength and higher energy barriers for self-diffusion. This explanation is supported by the two-body excess entropy behavior as it is known in the literature that disorder enhances the ability of atoms to diffuse[42–45].

The network connectivity (NC) is calculated using $NC = \sum_{n=1}^{4} x_n n$, where x_n is the fraction of the Q^n (n= 1, 2, 3, or 4) species and are calculated based on our previous study[3]. The NC represents the average number of bridging oxygen (BO) in the coordination shell of Si and/ or Al. Figure 5(a) depicts the network connectivity (NC) as a function of FS. The NC tend to decrease with increasing FS, indicating that the glass structure tends to be less polymerized when containing high FS modifiers. This could be another reason for the higher diffusion of charge balancing cations which indeed leads to a lower T_g[46]. Recently, many authors[47–50] used a theoretical structural descriptor named F_{net} to estimate the strength of the glass network. It is calculated by a summation of the cation—oxygen bonds and weighting them by the bond enthalpies (BE)[51] as shown in eq. 2

$$F_{net} = \frac{1}{N}\left[\sum_{i}^{cations}\sum_{j}^{anions} n_i CN_{ij} BE_{ij} m_{ij}\right] \quad (2)$$

with N standing for the total number of atoms, n_i is the number of atoms of the i-th type; CN_{ij} is the mean coordination number of ij pairs, i = Si, Al, Li, Na, K, Mg, Ca, Sr, Ba, Zn and j = O. BE_{ij} are the bond enthalpies, obtained from ref[51]. m_{ij} represents the maximum number of SiO_4 and AlO_4 units linked to i-O bonds and is used to evaluate better the contribution of each bond to the overall network strength and for this we used the values suggested in ref[48,49] and used previously in some papers[47–50]. Following these values, the number of Si—O bonds is multiplied by 4, Al—O by 4, alkali—O by 1, alkaline earth—O by 2, and Zn—O by 2. The effect due to the presence of Al in polyhedral states higher than 4 is neglected as the fraction of these elements is considerably lower than that of tetrahedral state. More details about the calculation of F_{net} could be found in refs[47–50]. The F_{net} parameter obviously takes into account both structural and energetic properties of the glass. Fig. 5(b) shows a correlation between F_{net} and T_g. From this figure, we can distinguish two distributions: one for alkali AS glasses and the other one for alkaline earth AS glasses. T_g was found to be positively correlated to F_{net} for both families, which is in good agreement with the literature cite. It is also worth stressing that the network connectivity increases with increasing F_{net} which is supporting our arguments.

The fragility is a scalar to quantifies the rate at which any dynamical quantity such as viscosity or diffusion grows with temperature[52–54]. The fragility of the liquid was computed from the Arrhenius behavior as in Refs.[28,55] (see supplementary materials Fig. S8). The values calculated here are in good agreement with the values reported in many experiments[39,56,57]. The high fragile nature of the alkaline earth aluminosilicate melts may result from the differences in the diffusion in these systems as compared to the alkali aluminosilicate melts. In contrast to the glass-forming melts with high fragility, the low fragility glass-forming melts show a relatively broad glass transition temperature range as they exhibit a relatively slow change in the viscosity with temperature, which gives more time for the glass-forming melts to relax its structure.

As we have noticed from the results presented herein, the pre-exponential factor D_0 and diffusion energy barrier E_a have an important contribution to the diffusion coefficient as for the activation energy governed by the ionic size and mass of the cation and by the structural configuration of the host medium. From the fitting of the diffusion data to the Arrhenius equation, we determine the values of D_0 and E_a and its contributions to the diffusion coefficients of the studied glasses. We found that the pre-exponential factor D_0 shows a correlation with FS as for the activation energies (see supplementary materials Fig. S9) Self-diffusion coefficient D can be expressed as

$$\begin{aligned} D = D^* exp(-\frac{G}{k_B T}) = D^* exp(\frac{S}{k_B}) exp(-\frac{H}{kT}) \\ = D_0 exp(-\frac{H}{k_B T}) \end{aligned} \quad (3)$$

where $D_0 = D^* exp(\frac{S}{k_B})$, G, H, and S denote the Gibbs free energy, enthalpy, and entropy of activation of the self-diffusion process, respectively, the pre-exponential factor and activation energy are dominated by entropy and enthalpy contributions. In the charge-balanced aluminosilicate glasses, the self-diffusion of cations is dominated by the base glass, which has different glass

View Article Online
DOI: 10.1039/D0CP02910F

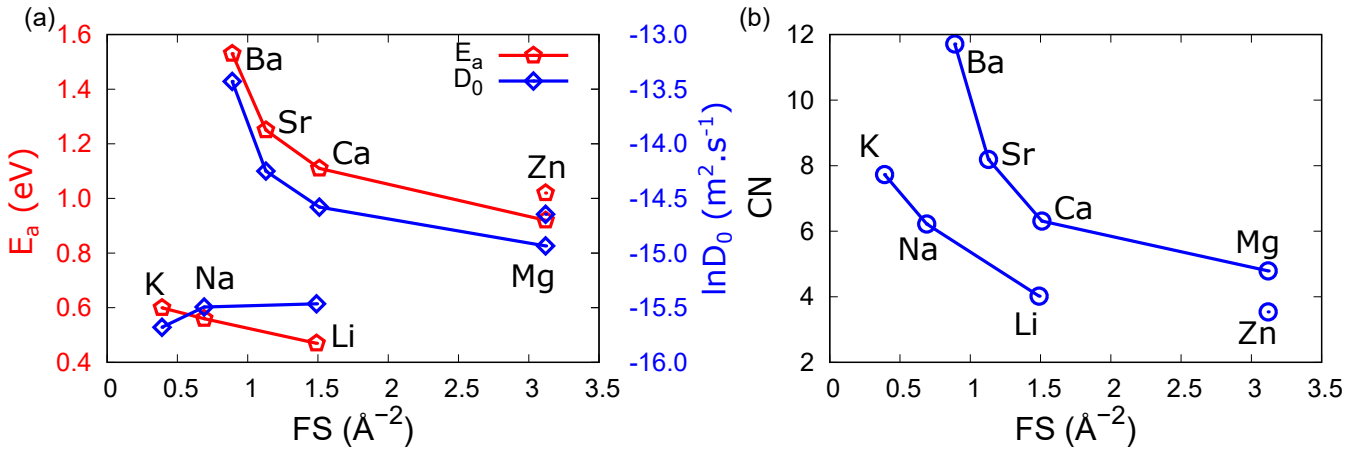

Fig. 4 (a) Activation energies E_a and pre-exponential factor D_0, of Li, Na, K, Mg, Ca, Sr, Ba, and Zn as a function of charge balancing cations field strength for the studied aluminosilicates. (b) mean coordination number of the charge balancing cations to oxygen as a function of FS in the studied aluminosilicates at 300 K. The symbols represent the simulated data points, and the lines are guide to the eye, error bars are smaller than the symbol size, and they are omitted from the plot.

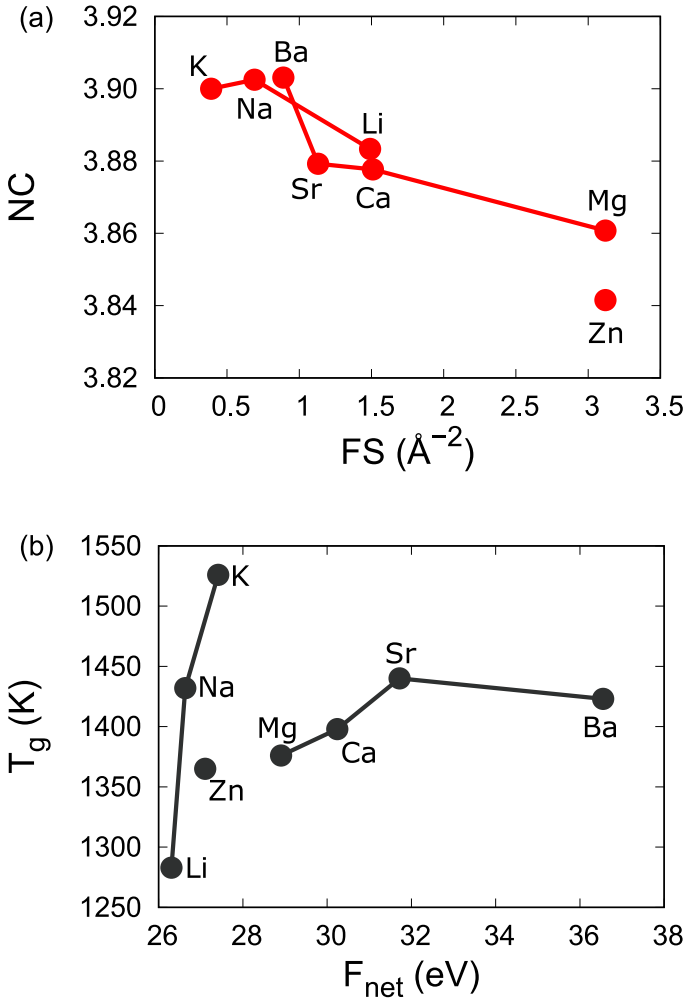

Fig. 5 (a) Network connectivity as a function of FS in the studied aluminosilicates at 300 K. (b) The glass transition temperature as a function of the F_{net}. The symbols represent the simulated data points, and the lines are guide to the eye.

structures, as shown by simulation results. This difference in the structure leads to different configurational and vibrational entropy and hence different activation entropy leading to different pre-exponential factors of diffusion. The pair excess entropy shows qualitatively that the configurational entropy of the studied melts is affected remarkably by the charge balancing cations.

5 Conclusion

Molecular dynamics simulations were performed to understand the origins of the anomalous behavior of T_g as a function of FS and the effect of the charge balancing cations on the diffusion behavior in the aluminosilicates. The results showed that the origins of this anomaly are linked to the diffusion of the charge balancing cations. The high FS cations diffuse faster than the low FS cations, and this behavior was attributed to the high pair excess entropy, which also indicates a high disorder. This high diffusion of the charge balancing cations allows for a relaxation of the structure, thus, exploring low energy minima, which leads to a low T_g. Additionally, the melt fragility showed that AS glasses with high field strength tend to be strong glass-forming melts (low fragility index) compared to the ones with high FS; the fragility of the alkaline earth aluminosilicate melts is also responsible for the differences in the diffusion in these systems as compared to the alkali aluminosilicate melts. Altogether the results presented in this letter will deepen our understanding of the role of different modifiers on the diffusion behavior in silicate and aluminosilicate (as the insight given here is expected to hold also for binary silicate systems) and help in getting an atomic-scale understanding of the glass transition.

Conflicts of interest

There are no conflicts to declare.

Acknowledgements

The authors gratefully acknowledge the computing resources provided by the Erlangen Regional Computing Center (RRZE) to run some of the simulations.

View Article Online
DOI: 10.1039/D0CP02910F

Notes and references

1 Y. Yu, M. Wang, D. Zhang, B. Wang, G. Sant and M. Bauchy, *Phys. Rev. Lett.*, 2015, **115**, 165901.

2 R. C. Welch, J. R. Smith, M. Potuzak, X. Guo, B. F. Bowden, T. J. Kiczenski, D. C. Allan, E. A. King, A. J. Ellison and J. C. Mauro, *Phys. Rev. Lett.*, 2013, **110**, 265901.

3 A. Atila, E. M. Ghardi, S. Ouaskit and A. Hasnaoui, *Phys. Rev. B*, 2019, **100**, 144109.

4 A. Dietzel, *Z ELKTROCHEM ANGEW P*, 1942, **48**, 9–23.

5 C. J. Wilkinson, E. Pakhomenko, M. R. Jesuit, A. DeCeanne, B. Hauke, M. Packard, S. A. Feller and J. C. Mauro, *J. Non. Cryst. Solids*, 2018, **502**, 172–175.

6 E. R. Barney, A. C. Hannon, D. Holland, N. Umesaki and M. Tatsumisago, *J. Non. Cryst. Solids*, 2015, **414**, 33–41.

7 N. S. Tagiara, E. Moayedi, A. Kyritsis, L. Wondraczek and E. I. Kamitsos, *J. Phys. Chem. B*, 2019, **123**, 7905–7918.

8 M. Zhang, S. Mancini, W. Bresser and P. Boolchand, *J. Non. Cryst. Solids*, 1992, **151**, 149 – 154.

9 C. Hermansen, B. P. Rodrigues, L. Wondraczek and Y. Yue, *J. Chem. Phys*, 2014, **141**, 244502.

10 K. Januchta, M. Bauchy, R. E. Youngman, S. J. Rzoska, M. Bockowski and M. M. Smedskjaer, *Phys. Rev. Materials*, 2017, **1**, 063603.

11 N. Mascaraque, K. F. Frederiksen, K. Januchta, R. E. Youngman, M. Bauchy and M. M. Smedskjaer, *J. Non. Cryst. Solids*, 2018, **499**, 264 – 271.

12 A. Pedone, G. Malavasi, A. N. Cormack, U. Segre and M. C. Menziani, *Theor. Chem. Acc*, 2008, **120**, 557–564.

13 C. Weigel, C. Le Losq, R. Vialla, C. Dupas, S. Clément, D. R. Neuville and B. Rufflé, *J. Non. Cryst. Solids*, 2016, **447**, 267–272.

14 H. Jabraoui, E. Achhal, A. Hasnaoui, J.-L. Garden, Y. Vaills and S. Ouaskit, *Journal of Non-Crystalline Solids*, 2016, **448**, 16–26.

15 A. Atila, E. M. Ghardi, A. Hasnaoui and S. Ouaskit, *J. Non. Cryst. Solids*, 2019, **525**, 119470.

16 A. Pedone, G. Malavasi, M. C. Menziani, A. N. Cormack and U. Segre, *J. Phys. Chem. B*, 2006, **110**, 11780–11795.

17 Y. Yu, M. Wang, N. M. Anoop Krishnan, M. M. Smedskjaer, K. Deenamma Vargheese, J. C. Mauro, M. Balonis and M. Bauchy, *J. Non. Cryst. Solids*, 2018, **489**, 16–21.

18 A. Atila, *Submitted*, 2020.

19 E. M. Ghardi, A. Atila, M. Badawi, A. Hasnaoui and S. Ouaskit, *J. Am. Ceram. Soc*, 2019, **102**, 6626–6639.

20 S. Plimpton, *J. Comput. Phys*, 1995, **117**, 1 – 19.

21 X. Li, W. Song, K. Yang, N. A. Krishnan, B. Wang, M. M. Smedskjaer, J. C. Mauro, G. Sant, M. Balonis and M. Bauchy, *J. Chem. Phys*, 2017, **147**, 074501.

22 F. Lodesani, M. C. Menziani, H. Hijiya, Y. Takato, S. Urata and A. Pedone, *Scientific reports*, 2020, **10**, 1–18.

23 S. Urata, *The Journal of Chemical Physics*, 2019, **151**, 224502.

24 J. Buchholz, W. Paul, F. Varnik and K. Binder, *J. Chem. Phys*, 2002, **117**, 7364–7372.

25 K. Vollmayr, W. Kob and K. Binder, *J. Chem. Phys*, 1996, **105**, 4714–4728.

26 J. Tan, S. Zhao, W. Wang, G. Davies and X. Mo, *Materials Science and Engineering: B*, 2004, **106**, 295 – 299.

27 C. M. Alvares, G. Deffrennes, A. Pisch and N. Jakse, *The Journal of Chemical Physics*, 2020, **152**, 084503.

28 M. Bauchy, M. Micoulaut, M. Boero and C. Massobrio, *Phys. Rev. Lett.*, 2013, **110**, 165501.

29 Y. Zhao, J. Du, X. Qiao, X. Cao, C. Zhang, G. Xu, Y. Liu, S. Peng and G. Han, *J. Non. Cryst. Solids*, 2020, **527**, 119734.

30 M. Micoulaut and M. Bauchy, *Phys. Rev. Lett.*, 2017, **118**, 145502.

31 M. Bauchy and M. Micoulaut, *Phys. Rev. Lett.*, 2013, **110**, 095501.

32 A. N. Novikov, D. R. Neuville, L. Hennet, Y. Gueguen, D. Thiaudière, T. Charpentier and P. Florian, *Chem. Geol.*, 2017, **461**, 115 – 127.

33 X. Wu and R. Dieckmann, *J. Non. Cryst. Solids*, 2011, **357**, 3797 – 3802.

34 M. Bauchy and M. Micoulaut, *Phys. Rev. B*, 2011, **83**, 184118.

35 H. Tanaka, H. Tong, R. Shi and J. Russo, *Nat. Rev. Phys*, 2019, **1**, 333–348.

36 R. E. Nettleton and M. S. Green, *J. Chem. Phys*, 1958, **29**, 1365–1370.

37 E. Giuffré, S. Prestipino, F. Saija, A. M. Saitta and P. V. Giaquinta, *J. Chem. Theory Comput*, 2010, **6**, 625–636.

38 P. M. Piaggi and M. Parrinello, *J. Chem. Phys*, 2017, **147**, 114112.

39 C. Romano, B. Poe, V. Mincione, K. U. Hess and D. B. Dingwell, *Chem. Geol.*, 2001, **174**, 115 – 132.

40 N. A., G. K. L., M. P and G. G. V., *Phys. Chem. Miner*, 1985, **11**, 284–298.

41 P. C. Hess, *Physical chemistry of magmas*, Springer, 1991, pp. 152–191.

42 M. Ren and J. Du, *J. Am. Ceram. Soc*, 2016, **99**, 2823–2833.

43 I. Avramov and A. Milchev, *J. Non. Cryst. Solids*, 1988, **104**, 253–260.

44 R. Kirchheim, *J. Non. Cryst. Solids*, 1983, **55**, 243–255.

45 J. Swenson and L. Börjesson, *Phys. Rev. Lett.*, 1996, **77**, 3569–3572.

46 M. Neyret, M. Lenoir, A. Grandjean, N. Massoni, B. Penelon and M. Malki, *Journal of Non-Crystalline Solids*, 2015, **410**, 74–81.

47 X. Lu, L. Deng, S. Gin and J. Du, *The Journal of Physical Chemistry B*, 2019, **123**, 1412–1422.

48 X. Lu and J. Du, *Journal of Non-Crystalline Solids*, 2020, **530**, 119772.

49 A. Pedone, X. Chen, R. G. Hill and N. Karpukhina, *The Journal of Physical Chemistry B*, 2018, **122**, 2940–2948.

50 G. Lusvardi, G. Malavasi, F. Tarsitano, L. Menabue, M. Menziani and A. Pedone, *The Journal of Physical Chemistry B*, 2009, **113**, 10331–10338.

51 J. Kerr, *CRC Handbook of Chemistry and Physics, 1st ed.; Lide, DR, Ed*, 2000.

View Article Online
DOI: 10.1039/D0CP02910F

52 A. Angell, *Nature*, 1998, **393**, 521–523.
53 K. Ito, C. T. Moynihan and C. A. Angell, *Nature*, 1999, **398**, 492–495.
54 A. Banerjee, M. K. Nandi, S. Sastry and S. M. Bhattacharyya, *J. Chem. Phys*, 2016, **145**, 034502.
55 M. Micoulaut, *J. Phys. Condens. Matter*, 2010, **22**, 285101.
56 M. Moesgaard and Y. Yue, *J. Non. Cryst. Solids*, 2009, **355**, 867 – 873.
57 T. K. Bechgaard, J. C. Mauro, M. Bauchy, Y. Yue, L. A. Lamberson, L. R. Jensen and M. M. Smedskjaer, *J. Non. Cryst. Solids*, 2017, **461**, 24 – 34.